



HAL
open science

CTH:YAG : from laser medium to luminescent concentrator

Lisa Lopez, Pierre Pichon, Frédéric Druon, Sophie Coumar, Clément Oriol,
Patrick Georges, François Balembois

► **To cite this version:**

Lisa Lopez, Pierre Pichon, Frédéric Druon, Sophie Coumar, Clément Oriol, et al.. CTH:YAG : from laser medium to luminescent concentrator. *Optics Express*, 2024, 32 (8), pp.14321. 10.1364/OE.515421 . hal-04723557

HAL Id: hal-04723557

<https://iogs.hal.science/hal-04723557v1>

Submitted on 7 Oct 2024

HAL is a multi-disciplinary open access archive for the deposit and dissemination of scientific research documents, whether they are published or not. The documents may come from teaching and research institutions in France or abroad, or from public or private research centers.

L'archive ouverte pluridisciplinaire **HAL**, est destinée au dépôt et à la diffusion de documents scientifiques de niveau recherche, publiés ou non, émanant des établissements d'enseignement et de recherche français ou étrangers, des laboratoires publics ou privés.



CTH:YAG : from laser medium to luminescent concentrator

LISA LOPEZ,* PIERRE PICHON, FRÉDÉRIC DRUON, 
SOPHIE COUMAR, CLÉMENT ORIOL, PATRICK GEORGES,  AND
FRANÇOIS BALEMBOIS

Université Paris-Saclay, Institut d'Optique Graduate School, CNRS, Laboratoire Charles Fabry, 91127, Palaiseau, France

*lisa.lopez@institutoptique.fr

Abstract: This work presents what we believe is a new way to use a CTH:YAG crystal for spontaneous emission instead of laser emission. The spontaneous emission is collected in one main direction thanks to a luminescent concentrator configuration. The CTH:YAG is indirectly LED-pumped by a Ce:YAG delivering 3.5 ms pulses at 10 Hz with an energy of 2 J in the visible (550–650 nm). In a configuration optimized for light extraction, the CTH:YAG luminescent concentrator provides a broadband emission between 1.8 μm and 2.1 μm with a unique combination of power (1 W) and brightness (21.2 $\text{W}/\text{cm}^2/\text{sr}$) that could be useful for short-wave infrared (SWIR) lighting applications.

© 2024 Optica Publishing Group under the terms of the [Optica Open Access Publishing Agreement](#)

1. Introduction

Cr,Tm,Ho:YAG (CTH:YAG) is an infrared laser medium known for many years [1,2]. Its emission at 2.1 μm is both in an atmospheric window and in the eye-safe region. This makes it attractive for remote sensing applications such as airborne Lidar [3,4]. In addition, its emission wavelength corresponds to a peak of water absorption, which is useful for medical applications. The ability of CTH:YAG to cut and ablate tissues is further enhanced by its ability to be transmitted through fused silica fibers. For example, CTH:YAG can be used for angioplasty, arthroscopy [5] or laser-induced kidney stone destruction [6]. In CTH:YAG, Ho^{3+} is responsible for laser emission at 2.1 μm , while Cr^{3+} and Tm^{3+} ions are used for pump absorption. Energy transfers from excited chromium and thulium ions are used to bring holmium ions to the upper $^5\text{I}_7$ level (Fig. 1(c)). The emission spectrum of CTH:YAG is not limited to 2.1 μm , but is broadband, between 1.7 μm and 2.15 μm [2], due to a combination of thulium and holmium fluorescence. Its emission covers much of the SWIR (Short Wavelength InfraRed) region, which is very useful for imaging applications, machine vision, biomedical imaging, or security. Such applications are growing with the advent of low-cost image sensors in the SWIR and require sources for illumination. To our knowledge, this very broad spectral band of CTH:YAG has never been exploited.

The use of spontaneous emission is well known in the visible with “laser phosphors” [7,8] using Ce doped crystals or ceramics pumped by blue laser diodes. In the near infrared, there are only a few reports on Ti:sapphire using a single-crystal fiber [9] and a square waveguide crystal [10], with output power limited to a few tens of mW in the near infrared. In the SWIR, erbium-doped fibers [11] or thulium-doped fibers [12] are well known as amplified spontaneous emission (ASE) sources. The output power can reach several hundred mW for a typical spectral bandwidth of 100 nm (full width at half maximum). Higher output powers have been achieved, but with reduced spectral bandwidth due to amplification by stimulated emission [13].

Apart fiber doped sources, spontaneous sources using SWIR “phosphors” are still under development [14]. Bulk materials started recently to be used for spontaneous emission. An Er:Yb:glass pumped by 64 LEDs at 940 nm emits a power of 980 mW with a brightness of 5 $\text{W}/\text{cm}^2/\text{sr}$ and a spectral bandwidth of 80 nm centered at 1550 nm [15]. An Er:Cr:YSGG

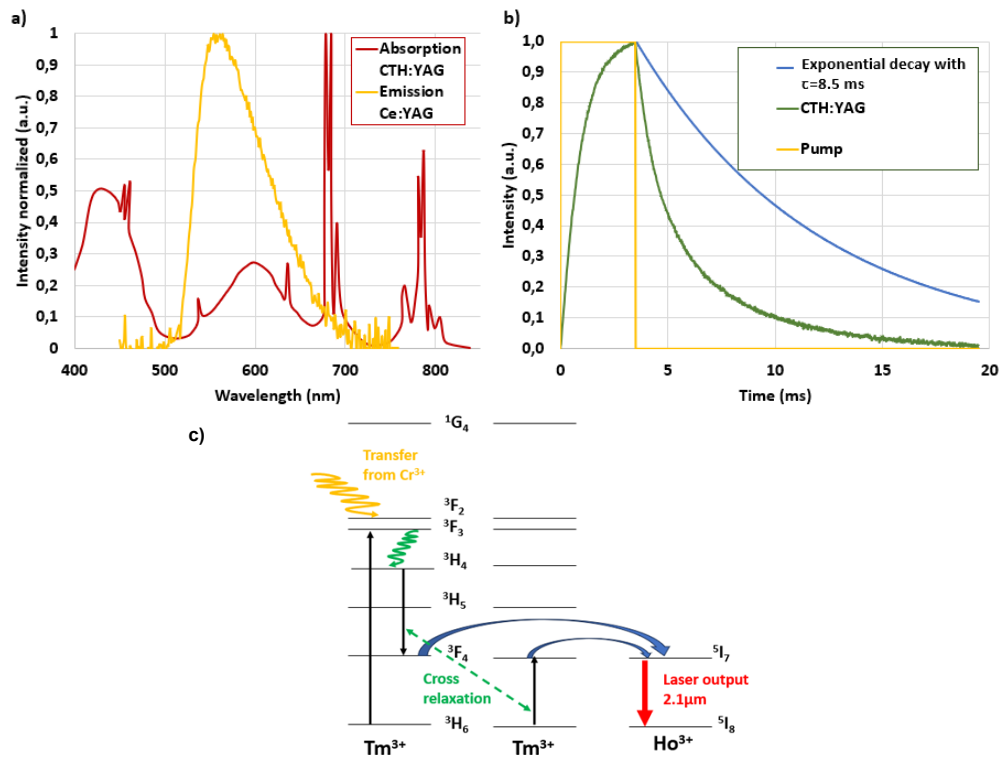


Fig. 1. a) Emission spectra of Ce:YAG concentrator (orange) and CTH:YAG absorption coefficient (red). b) Ce:YAG concentrator pump pulse and CTH:YAG emission in the SWIR pumped by the Ce:YAG. Comparison with an exponential decay of 8.5 ms corresponding to the lifetime of CTH:YAG [2]. c) Optical energy transfer between Cr, Tm, and Ho compositions of the CTH:YAG active medium. Cr and Tm absorb the flashlamp energy (direct pumping). Photon energy is also transferred from Cr (2E level) to Tm with 90% efficiency (indirect pumping).

indirectly LED-pumped by a Ce:YAG has produced a power of 350 mW with a brightness of 1.8 $\text{W}/\text{cm}^2/\text{sr}$ [16] with a broader spectral band of 200 nm centered at 1.6 μm . Therefore compared to the existing sources, the spontaneous emission CTH:YAG with a band of more than 300 nm between 1.7 μm and 2.15 μm has an interesting potential to cover a large part of the SWIR band with a single source.

In order to collect a maximum of spontaneous emission in one direction, we chose a luminescent concentrator architecture. This configuration uses an optically pumped parallelepiped with all its faces polished in order to trap and direct the spontaneous emission by total internal reflections towards the output face. This geometry has been inspired by the luminescent solar concentrators [17–20]. It has also been studied to generate new light sources in the visible with Ce:YAG luminescent concentrators [21–23] and recently in the SWIR with Er:Yb:glass [15] and Er:Cr:YSGG [16]. This paper reports the use of a CTH:YAG as a luminescent concentrator for the first time.

As a pump source, LEDs can be seen as an intermediate between flashlamps and laser diodes. They are inexpensive and very robust, like flashlamps. They also benefit from the long lifetime and stability of semiconductors. Recent advances in the lighting market make this pump source very attractive. CTH:YAG has already been diode pumped at 780 nm due to the strong absorption

band of Tm^{3+} [2,24]. In most cases, CTH:YAG is pumped by flashlamps taking advantage of the broad absorption of Cr^{3+} in the visible [1,25,26].

According to the absorption spectrum of CTH:YAG (Fig. 1(a)), pumping by blue LED seems to be possible due to the broad absorption of chromium ions. It could also be pumped by infrared LED around 800 nm, which corresponds to the narrow absorption line of thulium ions. In order to exploit the spontaneous emission of CTH:YAG, its spectroscopy must be taken into account. In fact, the transitions $^3\text{H}_6$ in thulium and $^5\text{I}_8$ in holmium are thermally populated (Fig. 1(c)). This results in a reabsorption loss coefficient of $\alpha=10^{-1} \text{ cm}^{-1}$ at 2.1 μm for the classical doping concentration (0.8 at. % for chromium, 6.0 at. % for thulium and 0.4 at. % for holmium) and for a visible pumping with flashlamp [25]. Therefore, to be efficient, the average propagation distance inside the CTH:YAG luminescent concentrator should be much smaller than $\frac{1}{\alpha}$, namely 10 cm. This means that the CTH:YAG dimensions should be in the order of a few centimeters. With such a small size, a CTH:YAG luminescent concentrator could be directly pumped by a few LEDs only. Since the power of a LED is in the order of one watt, the pump power would be severely limited in the case of direct LED pumping.

To avoid this problem induced by the low irradiance of the LED, we propose to investigate an indirect LED pumping by using a Ce:YAG luminescent concentrator as in [16]. In fact, Ce:YAG emits in a broadband (550-650 nm) with a good spectral overlap with the absorption of CTH:YAG (Fig. 1(a)). In addition, Ce:YAG luminescent concentrators pumped by blue LEDs have demonstrated power up to the kW level on small surfaces (14 mm \times 1 mm) in a quasi-continuous wave regime [27]. Therefore, the architecture chosen for this investigation is a cascade of luminescent concentrators: a LED-pumped Ce:YAG primary concentrator pumps a CTH:YAG secondary concentrator. This configuration has already been studied for solar harvesting [28].

After describing the experimental setup, the paper proposes original configurations of luminescent concentrators for thermal management and for power extraction. Finally, it compares the performance of the CTH:YAG luminescent concentrator with other incoherent sources emitting in the SWIR.

2. Experimental setup

In this study, we use a $3 \times 1 \times 14 \text{ mm}^3$ CTH:YAG crystal polished on all faces. It is provided by Electro-Optics Technology GmbH. Its concentration is holmium ions 0.36 at. %, chromium ions 0.85 at. % and thulium ions 5.9 at. %. As pump source, we chose a Ce:YAG luminescent concentrator pumped by blue LEDs. The Ce^{3+} concentration is $9.9 \cdot 10^{18} \text{ cm}^{-3}$ corresponding to an average absorption coefficient of 18 cm^{-1} over the LED emission spectrum. The blue LEDs have an emission spectrum centered at 450 nm (LUXEON Z Royal Blue from Lumileds). At a drive current of 1 A, each LED emits 900 mW over an area of $1 \times 1 \text{ mm}^2$. To avoid strong thermal effects in the LED panels, the LEDs operate in a quasi-continuous wave regime at 10 Hz with a pulse duration of 3.5 ms. This duration is limited by our electronic driver. Figure 1(b) shows the SWIR emission of CTH:YAG recorded by a photodiode. We use 2240 LEDs arranged in two panels of 1120 LEDs each with dimensions of $14 \times 200 \text{ mm}^2$. The concentrator consists of three $1 \times 14 \times 100 \text{ mm}^3$ Ce:YAG (from Crytur) polished on all sides and glued together by UV curing adhesive (ref. VBB-1 from Vitralit) to form a $1 \times 14 \times 300 \text{ mm}^3$ plate. This 300-mm-long slab is chosen for space reasons between the mechanics of the pump head and the mounts of the mirrors. The large faces of the concentrator are pumped by the LED panels (Fig. 2(a)). The thickness of the Ce:YAG concentrator (1 mm) is sufficient to absorb all the blue light from the LEDs and to ensure good mechanical handling of the assembly.

A dielectric mirror is placed on one of the $1 \times 14 \text{ mm}^2$ edges to collect more energy from the opposite side, which is considered the output side. When the LEDs are driven at 1A (10 Hz 3.5 ms), we measure a peak power of 216 W and an energy of 756 mJ (Joule meter ref ES120C

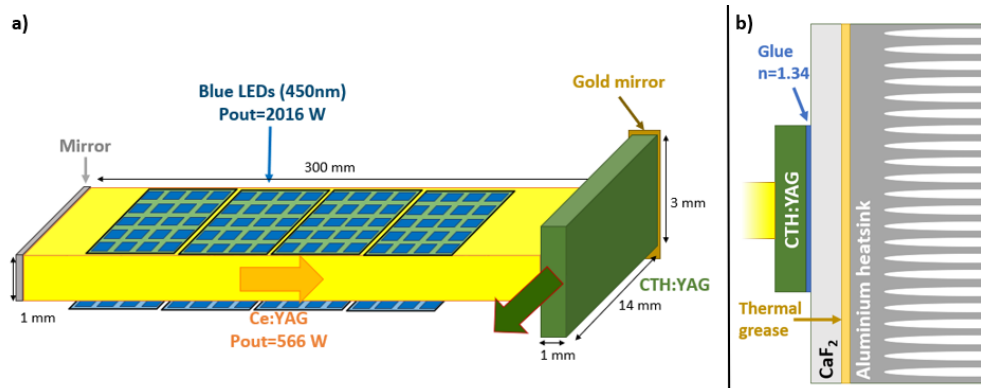


Fig. 2. a) LED-pumped CTH:YAG concentrator via a Ce:YAG luminescent concentrator. b) Schematic diagram of the device for optically bonded crystal cooling on a CaF₂ plate.

from Thorlabs) at the output of the Ce:YAG in the air resulting in an optical/electrical efficiency of 3.3%.

The CTH:YAG is bonded to the Ce:YAG at the center of its large area ($14 \times 3 \text{ mm}^2$) with UV-curing optical adhesive. Considering the refractive index of the adhesive ($n = 1.48$), we estimate that a peak power of $P_{pump} = 566 \text{ W}$ and an energy of 2 J are injected into the CTH:YAG. Under these experimental conditions (Fig. 2(a)), we measured an absorption of $Abs = 56\%$ with an integrating sphere. This low value can be attributed to the low doping concentration in chromium ions. However, it is worth noting that it is much higher than the absorption of 1 mm thick CTH:YAG placed in air. In fact, the light entering the CTH:YAG is Lambertian, so the average path in the concentrator is much higher than the crystal thickness. In addition, since Ce:YAG and CTH:YAG are bonded together (Fig. 2(a)), some of the light transmitted through the Ce:YAG cannot escape into the air and is therefore trapped by total internal reflection on the faces of the CTH:YAG. We have calculated that these trapped rays represent 63% of the light coupled into the CTH:YAG and have a high probability of being absorbed into the CTH:YAG.

At full pump power and at 10 Hz, the average absorbed pump power reaches 11.2 W which requires thermal management as discussed in the next section.

3. Thermal management by optical contact

We use a thermal camera to monitor the temperature of the CTH:YAG because the performance of the CTH:YAG is highly sensitive to temperature [24]. With a simple pulsed air cooling on the crystal, the temperature already reaches 160°C for a reduced pump pulse duration of $800 \mu\text{s}$ at 10 Hz (average absorbed pump power of 2.6 W), with the risk of burning the adhesive. To increase the average power, cooling with a heat sink is necessary. However, thermal contact is a problem for a luminescent concentrator. As explained in [15], contact with a heat sink, even on a small part of the surface, frustrates the total internal reflections and can decrease the efficiency of the luminescent concentrator significantly (by 40% in the case of [15]). The following is a solution for cooling without interfering with total internal reflection, thus maintaining light confinement in the luminescent concentrator.

In order to understand how the light is confined in the CTH:YAG concentrator and to master the frustration of total internal reflections, we propose a view in a planisphere [29], which represents the escape cones on different surfaces of the structure (Fig. 3). An escape cone contains the rays that are not trapped by total internal reflection at a given plane interface. Since the concentrator is a parallelepiped, there are 6 faces and thus 6 escape cones. The size of the escape cone depends

on the indices of the media at the interface: for an output in air (corresponding to the 4 disks in Fig. 3), the apex angle of the cone is 33.7° . For an interface between CTH:YAG and adhesive of $n = 1.48$, the apex angle is 55.3° (the upper band in Fig. 3 is the representation of the escape cone centred at $\beta=90^\circ$, for the first largest face). For an interface between CTH:YAG and an adhesive of $n = 1.34$, the apex angle is 48° (the lower band in Fig. 3 is the representation of the corresponding escape cone centred at $\beta=-90^\circ$, for the second largest face). Figure 3 shows that the different cones do not intersect. This means that an output in air is not affected by the frustration of total internal reflection induced by optical adhesive with a well-chosen refractive index. Therefore, the idea here is to replace an uncontrolled mechanical interface used for cooling with a well-controlled optical interface and to report the cooling to another interface in close proximity. This is done by contacting a CaF_2 plate (dimension $1 \times 20 \times 100 \text{ mm}^3$) with good thermal conductivity (9.7 W/m/K) to the adhesive on the one side and to the mechanical cooler on the other side via a thermal grease (Fig. 2(b)).

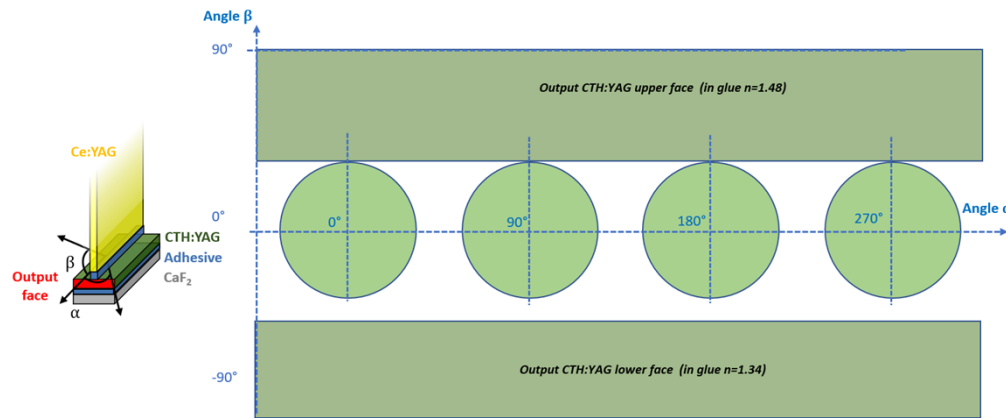


Fig. 3. Representation of the escape cones of the concentrator in a planisphere. The green disks correspond to CTH:YAG escape cones in air (33.7°)

Experimentally, we don't see any difference in the output power with or without gluing the CTH:YAG to the CaF_2 plate, as expected and explained with Fig. 3.

Figure 4 shows the temperature of the assembly for operation at 10 Hz, at full power and maximum pulse duration (3.5 ms). Thanks to the CaF_2 cooling, the temperature rise of the CTH:YAG is kept at an acceptable level of 110°C (Fig. 4(a)). One has to mention that the heating of Ce:YAG by the LED pumping is very low, thanks to its excellent conversion efficiency from the blue to the visible (88% [30]).

Despite the thermal management, the temperature remains high ($> 100^\circ\text{C}$) and may affect the performance of the CTH:YAG concentrator. In order to investigate this point, we estimate the loss coefficient α inside the luminescent concentrator by measuring the output power emitted from the output face with or without a gold mirror placed on the opposite face (see Fig. 2(a)). The output powers are denoted by P (without mirror) and P_m (with a mirror). The ratio $\frac{P_m}{P}$ can be related to the loss coefficient ([31]):

$$\frac{P_m}{P} = \frac{1 + R \cdot e^{-\alpha k l}}{1 + (1 - T) \cdot e^{-\alpha k l}} \cdot \frac{1 - e^{-2\alpha k l} \cdot (1 - T)^2}{1 - e^{-2\alpha k l} \cdot R \cdot (1 - T)} \quad (1)$$

with $k = \frac{-\ln(\cos \theta_{TIR})}{(1 - \cos \theta_{TIR})}$, θ_{TIR} is the apex angle of the escape cone in air ($\theta_{TIR} = 33.7^\circ$), T is the Fresnel transmission of the output interface taking all directions in the output escape cone and all polarizations into account ($T = 0.91$) and l is the length of the concentrator ($l = 14 \text{ mm}$) and R is the reflectivity of the gold mirror ($R = 97.5\%$).

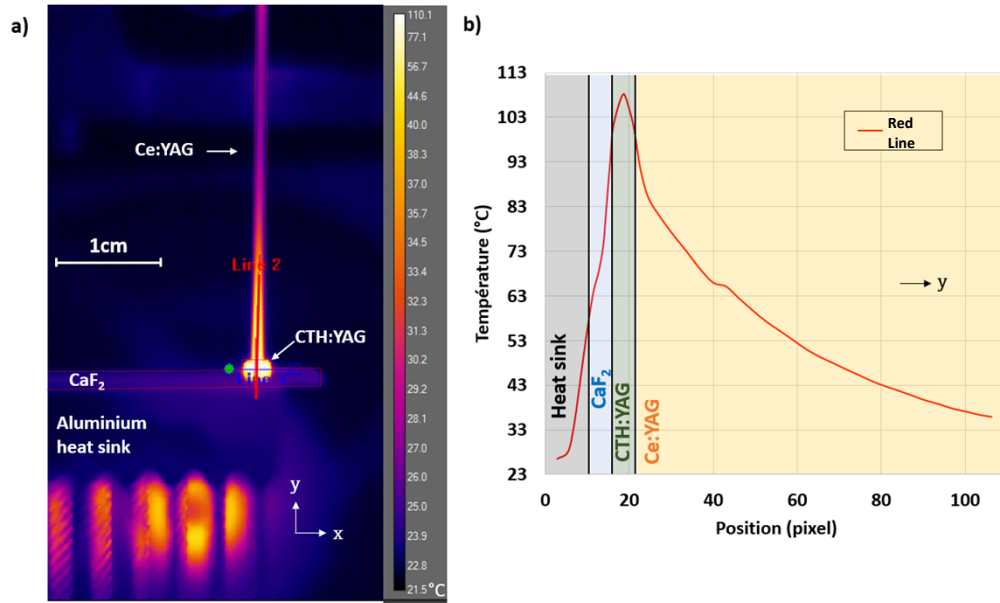


Fig. 4. a) Thermal camera photo of CTH:YAG crystal at 3.5 ms. b) Longitudinal section along the red line from the thermal camera photo.

We experimentally measure a ratio $\frac{P_m}{P} = 1.5$ with $P = 550$ mW and $P_m = 850$ mW, which leads to a loss coefficient of $\alpha = 0.37$ cm⁻¹ (at maximum average pump power for a temperature of 110°). This value is high compared to previous measurements (0.1 cm⁻¹ [25]) for similar doping levels. We attributed this effect to the temperature since the lower levels of transitions in thulium and holmium are thermally populated. This loss coefficient is very high compared to other luminescent concentrators (for Ce:YAG $\alpha < 10^{-2}$ cm⁻¹ [32]). This imposes to keep the propagation distance inside the CTH:YAG lower than $1/\alpha = 2.7$ cm. This justifies the dimensions of this CTH:YAG luminescent concentrator.

The optical efficiency $\frac{P}{P_{pump}}$ is analysed experimentally and theoretically in the simplest case ie. without a rear mirror. We measured a value $\frac{P}{P_{pump}} = 0.15\%$, which is quite low. To better understand this result, we use the formula giving the output power of the concentrator without rear mirror [29].

$$P = \frac{(1+(1-T)e^{-\alpha kl})}{1-(1-T)^2 e^{-2\alpha kl}} T \cdot \eta_r \frac{\lambda_p}{\lambda_{em}} Abs \frac{1-\cos\theta_{TR}}{2} \frac{1}{\alpha lk} (1 - e^{-\alpha lk}) P_{pump} \quad (2)$$

All parameters are given and explained in Table 1 and are known except for the fluorescence quantum yield η_r . Since its value has not been found in the literature and is highly dependent on the operating conditions of the CTH:YAG crystal, we decided to use it as a fitting parameter to match calculation and measurement. We then find $\eta_r = 17\%$. It is worth to note that this parameter takes our pumping conditions in account.

Table 1. CTH :YAG parameters

| Parameters | CTH :YAG (0.8 at. % chromium, 6.0 at. % thulium et 0.4 at. % et holmium) | Comments |
|-------------------------------------|--|--|
| Refractive index | $n = 1.8$ | Given at $2 \mu\text{m}$ |
| Pump wavelength (peak) | $\lambda_p = 580 \text{ nm}$ | Mean wavelength of the Ce:YAG |
| Absorption (Abs) | Abs = 56% | Measured with Ce :YAG spectrum |
| Emitted wavelength | $\lambda_{em} = 1 \text{ 927 nm}$ | Mean wavelength of the CTH:YAG |
| Propagation losses | $\alpha = 0.37 \text{ cm}^{-1}$ | |
| Thickness | $t = 1 \text{ mm}$ | |
| Width | $w = 3 \text{ mm}$ | |
| Length | $l = 14 \text{ mm}$ | |
| Fresnel transmission | $T = 0.91$ | Averaged over the two polarizations |
| Solid angle of exit cone in air | $\Omega_{air} = 1.06 \text{ sr}$ | $\Omega = 2\pi(1 - \cos\theta_{TIR})$ |
| Adhesive index | $n_{glue} = 1.48$ | Value specified by the manufacturer Vitralit |
| CPC index | $n_{cpc} = 1.52$ | Made of Schott B 270 glass |
| Solid angle of exit cone in the CPC | $\Omega_{CPC} = 2.71 \text{ sr}$ | $\Omega = 2\pi(1 - \cos\theta_{TIR})$ |

4. Light extraction

Figure 3 shows that only a small part of the spontaneous emission can be collected at the output: typically equal to 8% for the escape cone in air (without propagation losses). With a mirror on the opposite side, the fraction can be increased to 16% (without propagation losses). To improve the performance of the CTH:YAG, a Compound Parabolic Concentrator (CPC#17-709 from Edmund Optics, diameter₁ = 5.39 mm with an acceptance angle of 45° and diameter₂ = 2.5 mm) is bonded to the output surface (Fig. 6(a)) in a reverse orientation, as in [33]. Figure 5 shows that the adhesive (refractive index $n = 1.48$) between the CPC and the CTH:YAG allows a larger escape cone (apex angle 55.3°) than an escape cone in air (apex angle 33.7°). Because the CPC reduces the angle of the off-axis rays, the rays can escape through the output surface of the CPC. The CPC has been chosen such that its maximum etendue E_{max} is larger than the beam etendue E extracted from the CTH:YAG through the glue. The latter is $E = \pi \cdot n_{glue}^2 A_{in}$, where A_{in} is the input area of the CPC (2.5 mm diameter). At the output of the CPC, the maximum etendue is : $E_{max} = \pi \cdot A_{out} \sin^2 \alpha$, where A_{out} is the output area of the CPC (5.39 mm diameter) and α its acceptance angle (45°). Here, the ratio $\frac{E}{E_{max}} = \frac{\pi \cdot n_{glue}^2 A_{in}}{\pi \cdot A_{out} \sin^2 \alpha}$ has a value of 0.94 showing that the CPC does not limit the extraction of rays coming from the CTH:YAG.

Considering the Fresnel losses at the various interfaces and the transmission of the CPC in the SWIR band, and the imperfect overlap between the CPC surface (2.5 mm diameter) and the output surface ($1 \times 3 \text{ mm}^2$), we expect an improvement factor of 2.19 in output power. The data used for the theoretical values are given in the Table 1.

However, one must also take into account the rays that could leak in the Ce:YAG (area 1, Fig. 5) and the rays that could leak in the CaF₂ (area 2, Fig. 5). It is possible to show that the rays in area 1 are in total internal reflections on the Ce:YAG surfaces except for the surface glued to the CTH:YAG. Consequently, these rays should return to the CTH:YAG. This was validated experimentally by measuring the losses using the method described in section 3 (Eq. (1)). We found exactly the same loss coefficient with or without gluing the Ce:YAG to the CTH:YAG concentrator. The rays coupled in the CaF₂ (area 2) are lost due to the thermal grease, which frustrates total internal reflections in the CaF₂. By measuring the overlap between the cones,

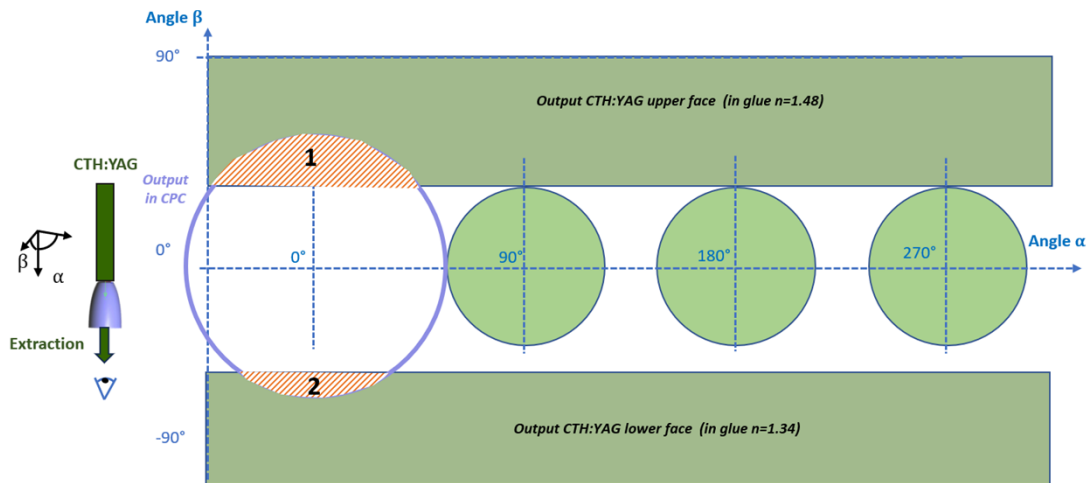


Fig. 5. Representation of the escape cones of the concentrator in a planisphere. The green cones correspond to CTH:YAG escape cones in air (33.7°). The escape cone of the CPC is in purple. The hatched area 1 corresponds to rays exiting the CTH:YAG through the upper face towards the Ce:YAG. The hatched area 2 corresponds to rays exiting the CTH:YAG through the lower face towards the CaF₂.

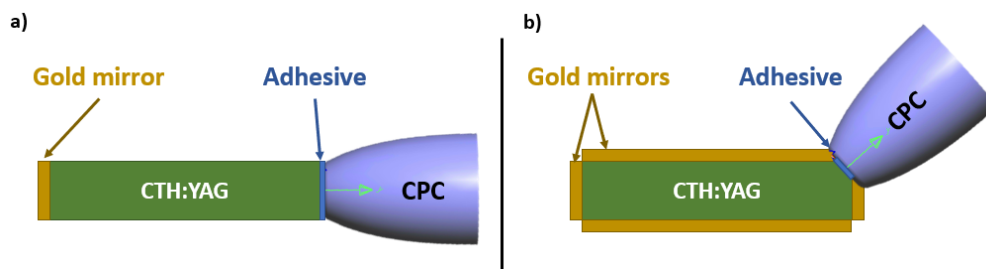


Fig. 6. Experimental set-up of the LED pumped CTH:YAG. View of the lower face $3 \times 14 \text{ mm}^2$. a) Straight configuration with glued CPC and a mirror at the back. b) Edge configuration with glued CPC and mirrors on the sides.

as shown in [29], we find a loss of 6% induced by this contact, which reduces the theoretical improvement by the CPC by a factor of 2.06 instead of 2.19.

Experimentally, the energy is measured with the Joulemeter and the temporal shape of the signal is used to trace the peak power (Fig 1(c)). A peak output power of 1.04 W is obtained with the CPC instead of 550 mW without (experiments done without the recycling gold mirror on the opposite face), giving an improvement factor of 1.9. The difference from the experimental value is partially due to the imperfect position of the CPC or an imperfect orientation of the CPC, which could increase the area 2.

In the configuration shown in Fig. 6(a), we measure a peak power of 1.28 W and an output beam diameter of 4 mm and a divergence of 80° (full width at half maximum). These characteristics are confirmed by LightTools simulations. This results in a peak luminance of 7.85 W/sr/cm^2 , which is already higher than that obtained in an Er:Yb luminescent concentrator (5.4 W/sr/cm^2) [15].

To further improve the performance, we polish an edge of $1 \times 1 \text{ mm}^2$ at 45° from the side faces (Fig. 6(b)), which acts as a new output face. It has its own escape cone, which is different from the other faces. This cone is imaged on the other sides faces in 3 multiple images that are

superimposed. In this way it is possible to collect 4 cones instead of 2 with a mirror at the back, as shown in Fig. 7. This configuration is called an “edge configuration” because we have added a new edge face to the structure. The 45° angle is the one that minimizes the overlap with the exit cones of the side faces.

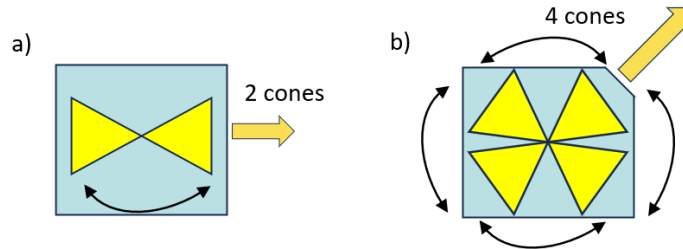


Fig. 7. Schematic diagram of cone collection for a) a conventional concentrator with two images of the output cone and b) an edge face concentrator with four images of the exit cone.

The same CPC as above is bonded to the additional surface as shown in Fig. 6(b). On the planisphere (Fig. 8) this corresponds to a new exit cone at 45° to the exit cones of the lateral faces (represented by the four disks). Experimentally, we found a peak output power of 700 mW in this configuration. This performance is lower than that of the Fig. 6(a) configuration for several reasons. First, Fig. 8 shows a strong overlap between the output cone and these escape cones. The calculation shows that it reaches 51%. In addition, the rays in this configuration travel a longer average distance that can be calculated [29]:

$$L_{edge} = \left(\frac{2\sqrt{2}w}{f} - 1 \right) \sqrt{2}l \quad (3)$$

where f is the length of the edge face, here 1 mm.

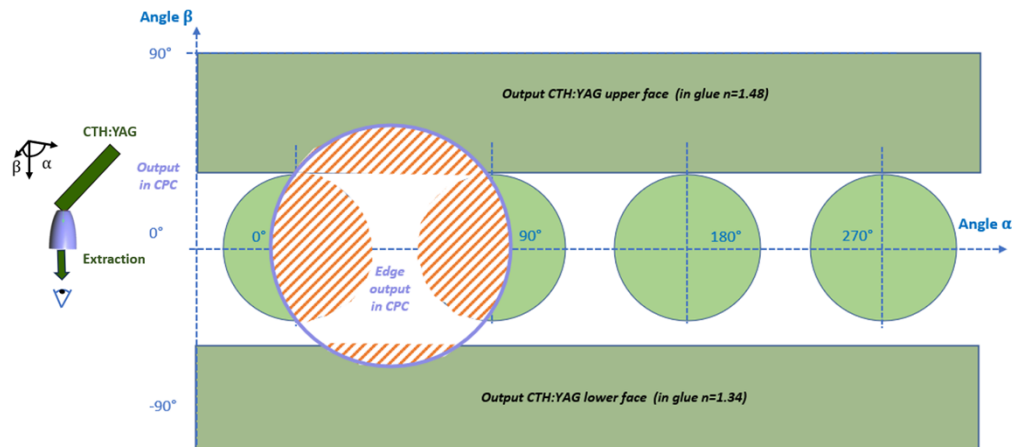


Fig. 8. Representation of the escape cones of the concentrator in a planisphere. The green cones correspond to CTH:YAG escape cones in air (33.7°). The escape cone of the CPC bonded to the edge face is in purple. The hatched areas correspond to rays exiting the CTH:YAG through other faces.

In our case $L_{edge} = 3.6 \text{ cm}$ that is larger than $1/\alpha$. This leads to propagation losses of 45%.





To recover the power lost on the escape cones of the lateral surfaces, we add gold mirrors to all the lateral surfaces. The power increases to 995 mW. This value is a little bit lower than expected

from the overlapping of the cones. Theoretically, an improvement factor of 1.46 is found close to the experimental value of 1.42. This can be explained by the imperfect recycling of the mirrors and also by the propagation losses in the CTH:YAG. Using LightTools we estimated that the output beam has a diameter of 2.8 mm and a divergence of 68° (full width at half maximum) corresponding to the reduced output area (1 mm^2) compared to the previous configuration (Fig. 6(a)). The divergence was confirmed experimentally by scanning the different angles with a photodiode. In summary, this edge-cut configuration demonstrated a peak luminance of $21.2 \text{ W/cm}^2/\text{sr}$. The luminance is strongly improved compared to the previous configuration. This is due to the light confinement in the three dimensions of space and to light recycling [32].

5. Discussion

Table 2 summarizes the performance achieved in the different configurations tested. It shows that the light extracted from the CTH:YAG is far from the ideal case (ie 8% in configuration A and 16% in configuration B) because of the high losses in our material. It also shows the interest to use a CPC for light extraction and an additional edge face for brightness enhancement. In all configurations, the peak output power remains directly proportional to the peak pump power, demonstrating that there is no sign of amplified spontaneous emission.

Table 2. Overview of the different configurations and their experimental performance. The percentage of light extraction from the CTH :YAG corresponds to the percentage of rays emitted by the CTH :YAG that are successfully extracted.

| | Configuration | Percentage of CTH:YAG light extraction | Luminance ($\text{W/cm}^2/\text{sr}$) | Peak power (mW) |
|---|---|--|---|-----------------|
| A |  | 5.9% | 5.36 | 550 |
| B |  | 9.7% | 8.86 | 835 |
| C |  | 13.7% | 7.85 | 1280 |
| D |  | 10.7% | 21.2 | 995 |




The performance of our CTH:YAG luminescent concentrator in configuration D can be compared with other sources. Table 3 compares this work with previously developed SWIR luminescent concentrators (Er:Yb:glass and Er:Cr:YSGG). It can be seen that our CTH:YAG concentrator achieves the best performance in terms of power and luminance.

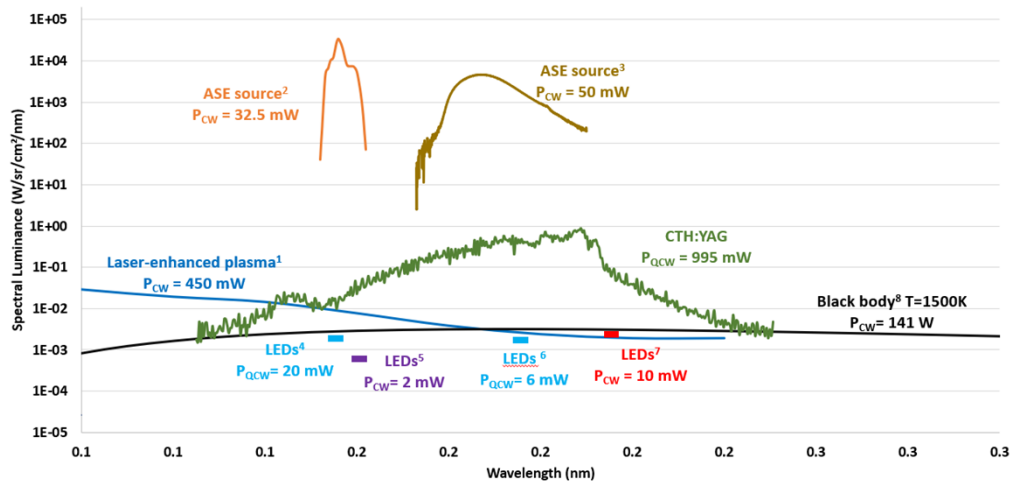
Next, the performance of the CTH:YAG is compared to other SWIR emitting sources in terms of spectral luminance and power (Fig. 9). The spectral luminance of the CTH:YAG is two orders of magnitude better than commercial LEDs and then a black body at 1500 K. It remains far below that of the Er-doped and Tm-doped fiber ASE sources. However, its peak power is 20 times higher, and its emission band is much wider (300 nm FWHM).

The efficiency (ratio of the peak output power over the peak pump) of CTH:YAG as a luminescent concentrator is 0.17%. This very low value must be compared with the efficiency of the CTH:YAG laser under flashlamp pumping, which is typically about 1% [25].

As a first explanation, Fig. 1(b) shows that the real lifetime of the Ho^{3+} ions is well below 8.5 ms [2] at full pump power. The decay rate is five times higher than the fluorescence decay rate related to the lifetime of CTH:YAG. This can be partly explained by a strong energy up-conversion transfer involving both thulium and holmium: for Tm^{3+} it is related to the conversion of two

Table 3. Comparison of CTH:YAG performance with other SWIR luminescent concentrators (peak emission wavelength is given in the first column)

| Crystal | Power | Luminance | Configuration |
|--|--------|-------------------------------------|--|
| Er:Yb:glass [15] (1.55 μm) | 850 mW | 5 $\text{W}/\text{cm}^2/\text{sr}$ |  |
| Er:Cr:YSGG [16] (1.6 μm) | 350 mW | 2 $\text{W}/\text{cm}^2/\text{sr}$ |  |
| CTH:YAG [this work] (2 μm) | 995 mW | 21 $\text{W}/\text{cm}^2/\text{sr}$ |  |

**Fig. 9.** State of the art of incoherent sources spectral luminance in the SWIR. P corresponds to the average power for continuous sources and to the peak power for quasi-continuous sources. The CTH:YAG experimental setup corresponds to the configuration D.

Tm^{3+} in ${}^3\text{F}_4$ to one ${}^3\text{H}_4$ Tm^{3+} and one ground state Tm^{3+} (${}^3\text{H}_6$). In addition, the ${}^3\text{F}_4$ Tm^{3+} and ${}^5\text{I}_7$ Ho^{3+} pair is being converted to a Tm^{3+} ground state and a ${}^5\text{I}_6$ Ho^{3+} . These effects play a key role in the low value of η_r [2]. This is also confirmed by the strong heating of the crystal, related with strong non radiative transitions. In contrast to laser operation, the efficiency of the luminescent concentrator is directly proportional to the population of the upper state level. Therefore, it is more sensitive than a CTH:YAG laser to the effects that limit the upper-state population.

Although this laser crystal is certainly not optimized for a luminescence concentrator, we show that it is manageable by appropriate thermal management, good choice of dimensions and optimization of extraction.

For further optimization, one must deal with two limitations revealed in this work. The first one comes from the upper level population, which is limited by up-conversion effects associated with strong non-radiative transitions and hence strong heating. From Fig. 1(b) we can deduce that the up-conversion rate is five times the spontaneous emission rate. The up-conversion can be limited by reducing the pump power density with a larger Ce:YAG (3 mm instead of 1 mm) and thus decreasing the population density of the upper state level. In addition, a lower concentration of Tm and Ho could also reduce the up-conversion parameter. The second limitation comes from

the losses induced by the thermally populated lower levels of the transitions, also a consequence of the temperature rise. Lowering the temperature through better cooling (sapphire instead of CaF₂, thermo-electric cooler instead of air cooling) could limit the reabsorption losses. In addition, a lower doping concentration in Tm and Ho could also help to reduce the reabsorption losses. The potential here is to double the output power of the edge configuration. Therefore, an optimized CTH:YAG could improve the performance by an order of magnitude.

In conclusion, this paper shows that a laser material like CTH:YAG can be efficiently redirected as a luminescent concentrator. It shows original solutions for thermal management and luminance enhancement associated with power extraction. It offers a unique combination of power (1 W) and brightness (21.2 W/cm²/sr) that is the highest of any luminescent concentrator in the SWIR. In addition, the indirect LED pumping by Ce:YAG provides high peak power and high luminance with all the advantages of semiconductors (lifetime and stability) and flashlamps (robustness and low cost). This kind of pumping could be a major key for robust, reliable SWIR sources for lighting applications.

Funding. Agence de l'innovation de Défense; Agence Nationale de la Recherche (project NewLight ANR-21-CE08-0044).

Disclosures. The authors declare no conflicts of interest.

Data Availability. Data underlying the results presented in this paper are not publicly available at this time but may be obtained from the authors upon reasonable request.

References

1. A. N. Allat'ev, E. V. Zharikov, S. P. Kalitin, *et al.*, "Lasing of holmium ions as a result of the ⁵I₇ → ⁵I₈ transition at room temperature in an yttrium scandium gallium garnet crystal activated with chromium, thulium, and holmium ions," *Sov. J. Quantum Electron.* **16**(10), 1404–1405 (1986).
2. T. Y. Fan, G. Huber, R. L. Byer, *et al.*, "Spectroscopy and diode laser-pumped operation of Tm,Ho:YAG," *IEEE J. Quantum Electron.* **24**(6), 924–933 (1988).
3. S. Guch and D. P. Stanley, "Lasers for airborne applications," in (1992), p. 1026904.
4. R. Targ, M. J. Kavaya, R. M. Huffaker, *et al.*, "Coherent lidar airborne windshear sensor: performance evaluation," *Appl. Opt.* **30**(15), 2013 (1991).
5. S. P. Wright, E. J. Adamkiewicz, P. F. Moulton, *et al.*, eds. (1992), pp. 54–58.
6. F. Strittmatter, M. Eisel, R. Brinkmann, *et al.*, "Laser-induced lithotripsy: a review, insight into laboratory work, and lessons learned," *Transl Biophotonics* **2**(1-2), e201900029 (2020).
7. N. Rondelez, A. Correia, W. Ryckaert, *et al.*, "Efficient transmissive remote phosphor configuration for a laser-driven high-luminance white light source," *Opt. Express* **30**(4), 5107 (2022).
8. Y. H. Song, E. K. Ji, B. W. Jeong, *et al.*, "High power laser-driven ceramic phosphor plate for outstanding efficient white light conversion in application of automotive lighting," *Sci. Rep.* **6**(1), 31206 (2016).
9. S.-C. Wang, T.-I. Yang, D.-Y. Jheng, *et al.*, "Broadband and high-brightness light source: glass-clad Ti:sapphire crystal fiber," *Opt. Lett.* **40**(23), 5594 (2015).
10. D. Sacchet, M. Brzezinski, J. Moreau, *et al.*, "Motion artifact suppression in full-field optical coherence tomography," *Appl. Opt.* **49**(9), 1480 (2010).
11. J. H. Lee, U.-C. Ryu, and N. Park, "Passive erbium-doped fiber seed photon generator for high-power Er³⁺-doped fiber fluorescent sources with an 80-nm bandwidth," *Opt. Lett.* **24**(5), 279 (1999).
12. Z. Y. Hu, P. Yan, Q. Liu, *et al.*, "High-power single-stage thulium-doped superfluorescent fiber source," *Appl. Phys. B* **118**(1), 101–107 (2015).
13. J. Aubrecht, P. Peterka, P. Honzátko, *et al.*, "Broadband thulium-doped fiber ASE source," *Opt. Lett.* **45**(8), 2164 (2020).
14. Y. Zhang, S. Miao, Y. Liang, *et al.*, "Blue LED-pumped intense short-wave infrared luminescence based on Cr³⁺-Yb³⁺-co-doped phosphors," *Light: Sci. Appl.* **11**(1), 136 (2022).
15. P. Pichon, J.-P. Blanchot, F. Balembois, *et al.*, "New LED-based high-brightness incoherent light source in the SWIR," *Opt. Express* **26**(7), 9353 (2018).
16. L. Lopez, F. Druon, P. Georges, *et al.*, "LED-pumped Er:Cr:YSGG light sources," *Opt. Express* **31**(17), 27604 (2023).
17. S. Dottermusch, T. Masuda, M. Endo, *et al.*, "Solar pumping of fiber lasers with solid-state luminescent concentrators: design optimization by ray tracing," *Adv. Opt. Mater.* **9**(12), 2100479 (2021).
18. Y. Liu, J. Keil, V. E. Ferry, *et al.*, "Energy and thermal performance analysis of quantum dot luminescent solar concentrators in greenhouses (Adv. Sustainable Syst. 8/2023)," *Adv. Sustainable Syst.* **7**(8), 2370027 (2023).
19. I. Papakonstantinou, M. Portnoi, and M. G. Debye, "The hidden potential of luminescent solar concentrators," *Adv. Energy Mater.* **11**(3), 2002883 (2021).

20. M. G. Debije and P. P. C. Verbunt, "Thirty years of luminescent solar concentrator research: solar energy for the built environment," *Adv. Energy Mater.* **2**(1), 12–35 (2012).
21. J. Sathian, N. Alford, and M. Oxborrow, "Intense, highly-efficient solid-state yellow light source based on rare-earth-doped luminescent concentrator," in (2015).
22. S. Roelandt, Y. Meuret, D. K. G. De Boer, *et al.*, "Incoupling and outcoupling of light from a luminescent rod using a compound parabolic concentrator," *Opt. Eng.* **54**(5), 055101 (2015).
23. A. Barbet, A. Paul, T. Gallinelli, *et al.*, "Light-emitting diode pumped luminescent concentrators: a new opportunity for low-cost solid-state lasers," *Optica* **3**(5), 465 (2016).
24. Z. Lin, C. Gao, M. Gao, *et al.*, "Diode-pumped single-frequency microchip CTH:YAG lasers using different pump spot diameters," *Appl. Phys. B* **94**(1), 81–84 (2009).
25. S. R. Bowman, M. J. Winings, R. C. Y. Auyeung, *et al.*, "Laser and spectral properties of Cr, Tm, Ho:YAG at 2.1 μm ," *IEEE J. Quantum Electron.* **27**(9), 2142–2149 (1991).
26. S. Imai, T. Yamada, Y. Fujimori, *et al.*, "A 20 W Cr³⁺, Tm³⁺, Ho³⁺: YAG laser," *Opt. Laser Technol.* **22**(5), 351–353 (1990).
27. P. Pichon, A. Barbet, J.-P. Blanchot, *et al.*, "LED-pumped alexandrite laser oscillator and amplifier," *Opt. Lett.* **42**(20), 4191 (2017).
28. S. Flores Daorta, A. Proto, R. Fusco, *et al.*, "Cascade luminescent solar concentrators," *Appl. Phys. Lett.* **104**(15), 153901 (2014).
29. P. Pichon, L. Lopez, M. Nourry-Martin, *et al.*, "Light extraction and brightness enhancement of luminescent rectangular slabs," *Advanced Photonics Research* **3**(7), 2100356 (2022).
30. J. Sathian, J. D. Breeze, B. Richards, *et al.*, "Solid-state source of intense yellow light based on a Ce:YAG luminescent concentrator," *Opt. Express* **25**(12), 13714 (2017).
31. L. Lopez, P. Pichon, P. Loiseau, *et al.*, "Ce:LYSO, from scintillator to solid-state lighting as a blue luminescent concentrator," *Sci Rep* **13**(1), 7199 (2023).
32. P. Pichon, F. Balembois, F. Druon, *et al.*, "3D luminescent concentrators," *Opt. Express* **29**(5), 6915 (2021).
33. D. K. G. De Boer and L. Haenen, "Extraction optics for high lumen density sources," *J. Eur. Opt. Soc.-Rapid Publ.* **15**(1), 8 (2019).